IEEE Access
Multidisciplinary | Rapid Review | Open Access Journal

Received March 16, 2019, accepted March 29, 2019, date of publication April 4, 2019, date of current version April 16, 2019.

Digital Object Identifier 10.1109/ACCESS.2019.2908993

Temperature Rise Simulation of Medium Voltage Cubicle Type Gas Insulated Switch-Gear Based on Coupling of Multi-Physical Fields

LIJUN WANG, (Senior Member, IEEE), RUI WANG, XIAOLIN LI, AND CHAO YAN
State Key Laboratory of Electrical Insulation and Power Equipment, Xi'an Jiaotong University, Xi'an 710049, China
Corresponding author: Lijun Wang (lijunwang@mail.xjtu.edu.cn)

This work was supported by the National Key R&D Program of China under Grant 2018YFB0904300.

ABSTRACT Usage of Cubicle type Gas-Insulator Switch-gear (C-GIS) is gradually increasing in power system. During the operation of C-GIS, long-term excessive temperature rise leads to degeneration of insulation and mechanical property, which may finally leads to fatal accidents. In order to analyze the temperature distribution of the C-GIS, the model of a 40.5 kV medium voltage SF_6 insulated C-GIS has been established and simulations based on electromagnetic-fluid-temperature coupling are carried out. In the simulations, eddy-current filed is solved by ansys-multiphysics to obtain the heat generation inside the C-GIS. In order to improve calculation accuracy, the contact resistance is taken into consideration and the physical characteristics of SF_6 gas are considered to be related to the temperature. First, simulations with and without surrounding air environment considered are carried out and the results are compared. The type test of temperature rise is also conducted to verify the simulation results. The simulation results are found out in agreement with experimental results. Second, in order to reduce the temperature rise and improve the design of C-GIS, recommendations are put forward. The influence of the cooling system and surrounding barriers is analyzed by numerical simulation.

INDEX TERMS Temperature rise simulation, cubicle type gas insulated switch-gear, multi-physical fields.

I. INTRODUCTION

As protective and control equipment in the electrical power systems, switching device is a kind of important transmission and distribution device. To maintain safe and stable operation of switching devices, excessive temperature rise has to be avoided. The research on the distribution of temperature in the switchgear is of great importance for the optimum design and improvement of service life of switchgear.

Along with the improvement of computer performance, a lot of researches on the temperature rise of electrical equipment using finite-element method are conducted. At first, these researches are all conducted based on electromagnetic-thermal coupling, in which the fluid field is ignored. Kawase *et al.* [1] established and analyzed the distribution of temperature by using three dimensional (3D) finite-element method and verified the simulation results by experiments. 3D model of low-voltage switching device with contact resistance considered are established by Paulke *et al.* [2] and thermal analysis of different operating status are analyzed. Monnier *et al.* [3] conducted numerical simulation on the spherical electrical contact, in which a two dimensional (2D) symmetrical model with material characteristics varying with temperature is established. Clemens *et al.* [4] conducted a numerical modeling of the electromagnetic and temperature field by finite element method. Mateev *et al.* [5] used Ansys to conduct an analysis of the electromagnetic and temperature field of the vacuum interrupter in high voltage switchgear. Mateev uses the result of the electromagnetic field as the heat source and then obtained the temperature distribution in the vacuum interrupter.

Though widely used, in the calculation of these researches, experienced values have to be applied to the boundary conditions. Due to the difference between the experienced values and the actual value, the accuracy of the simulations is affected. In consideration of this issue, Computational Fluid Dynamics (CFD) method which is of higher accuracy is introduced to simulate the temperature rise in the switching devices. With a 2D model, Kim *et al.* [6] applied electromagnetic-temperature-fluid coupled simulation to predict temperature rise of the extra-high voltage SF_6

The associate editor coordinating the review of this manuscript and approving it for publication was Xue Zhou.

2169-3536 © 2019 IEEE. Translations and content mining are permitted for academic research only.
Personal use is also permitted, but republication/redistribution requires IEEE permission.
See http://www.ieee.org/publications_standards/publications/rights/index.html for more information.

insulated switchgear bus bar. In the simulation, the Nusselt number is assumed constant and model geometry is applied to calculate the heat-transfer coefficients on the boundaries. With Ansys and CFX coupling, Pawar *et al.* [7] presented a simulation to analyze the temperature distribution of a high-voltage SF_6 insulated circuit breaker in 2012. They conducted simulations under 1000A and 2000A rated current and verified the simulations with experiments. Based on the validated model, temperature rise of the circuit breaker under 3150A is further predicted. In 2014, Wu *et al.* [8] analyze the distribution of temperature in a three-phase gas-insulated bus bar by electromagnetic-fluid-temperature coupled method. In their simulation, the thermal conductivity and viscosity of SF6 gas is obtained by Sutherland's law. Dhotre *et al.* [9] established an electromagnetic-fluid-temperature simulation to analyze the temperature rise of a high-voltage circuit breaker with HADAPT-FLUENT coupling. Taking advantage of the symmetrical structure of breaker, they simplified the model of the breaker by employing a symmetric boundary. Wang *et al.* [10] has simulated the medium voltage air-insulated switchgear based on electromagnetic-fluid-temperature field model. In their later research work, they analyzed the advantage and disadvantage between Ansys Apdl-Cfx and Maxwell-Fluent coupling methods [11].

In this paper, an electromagnetic-fluid-temperature multi-physical coupled field simulation of a 40.5 kV SF_6-insulated C-GIS is conducted. In the simulation, the coupling method between Ansys Multiphysics and Cfx is adopted to simulate temperature distribution of the C-GIS. To ensure higher accuracy, contact resistance is taken into consideration and the physical properties of the C-GIS are set as temperature-varying in the simulations. Experiment is later carried out, by which the simulation is validated. Based on the validated model, the influences of cooling system and surrounding barriers are analyzed by simulations in order to reduce the temperature rise of the C-GIS. These simulations can provide theoretical guidance to the reduction of temperature rise in switch-gear.

II. SIMULATION MODEL AND EQUATIONS

A. EQUATIONS OF EDDY-CURRENT FIELD

When alternating currents flow through the conductors, the time-varying electric currents generate time-varying magnetic fields and time-varying magnetic fields generate time-varying electric fields, which leads to eddy currents in return. Maxwell equations can describe this phenomenon accurately. Maxwell equations are formed by four equations, which are the Ampere circuital theorem, Faraday's law of electromagnetic induction, Gauss electric flux law and Gauss magnetic flux law:

$$\nabla \times \vec{\boldsymbol{H}} = \vec{\boldsymbol{J}} + \frac{\partial \vec{\boldsymbol{D}}}{\partial t} \tag{1}$$

$$\nabla \times \vec{\boldsymbol{E}} = -\frac{\partial \vec{\boldsymbol{B}}}{\partial t} \tag{2}$$

$$\nabla \cdot \vec{\boldsymbol{D}} = \rho \tag{3}$$

$$\nabla \cdot \vec{\boldsymbol{B}} = 0 \tag{4}$$

in which $\vec{\boldsymbol{H}}$ is the magnetic intensity vector, $\vec{\boldsymbol{J}}$ is the current density vector, $\vec{\boldsymbol{D}}$ is the electric displacement vector, $\vec{\boldsymbol{E}}$ is the electric intensity vector, $\vec{\boldsymbol{B}}$ is the magnetic flux density vector.

In this paper, Ansys Multiphysics is used to calculate ohmic losses. In Ansys Multiphysics solver, quasi-static electromagnetic field is applied to analyze the C-GIS. For quasi-static electromagnetic field, the electric displacement vector is ignored. The differential equations are listed below:

$$\nabla \times \vec{\boldsymbol{H}} = \vec{\boldsymbol{J}} \tag{5}$$

$$\nabla \times \vec{\boldsymbol{E}} = -\frac{\partial \vec{\boldsymbol{B}}}{\partial t} \tag{6}$$

$$\nabla \cdot \vec{\boldsymbol{B}} = 0 \tag{7}$$

The auxiliary equations are:

$$\vec{\boldsymbol{J}} = \sigma \vec{\boldsymbol{E}} \tag{8}$$

$$\vec{\boldsymbol{B}} = \mu \vec{\boldsymbol{H}} \tag{9}$$

in which μ is the permeability (H/m) and σ is the electrical conductivity ($1/\Omega\ m$).

In the calculation, the magnetic vector potential $\vec{\boldsymbol{A}}$ is introduced:

$$\vec{\boldsymbol{B}} \nabla \times \vec{\boldsymbol{A}} \tag{10}$$

Combining (5) and (10), the governing equation is introduced:

$$\nabla \times \frac{1}{\mu}(\nabla \times \vec{\boldsymbol{A}}) = \vec{\boldsymbol{J}} = \vec{\boldsymbol{J}}_s + \vec{\boldsymbol{J}}_e \tag{11}$$

in which $\vec{\boldsymbol{J}}_{\mathbf{s}}$ is the source current density vector, $\vec{\boldsymbol{J}}_{\mathbf{e}}$ is the eddy current density vector.

The eddy current density vector in the conducting material is:

$$\vec{\boldsymbol{J}}_e = \sigma \vec{\boldsymbol{E}} = -\sigma \frac{\partial \vec{\boldsymbol{A}}}{\partial t} \tag{12}$$

From (12), the governing equation can be wrote as:

$$\nabla \times \frac{1}{\mu}(\nabla \times \vec{\boldsymbol{A}}) = \vec{\boldsymbol{J}}_s - \sigma \frac{\partial \vec{\boldsymbol{A}}}{\partial t} \tag{13}$$

After calculation, the losses generated in the conductors can be obtained as follow:

$$\mathbf{P} = \frac{1}{2\sigma} \int_V \mathbf{J} \cdot \mathbf{J}^* d\mathbf{V} \tag{14}$$

B. EQUATIONS OF TEMPERATURE FIELD

Ohmic losses are continually generated and turn into heat during the normal operation of switch-gear, which leads to the temperature rise of conductors, shells and insulation. Thermal balance will be established after the difference between components and cooling medium has become steady. There are three kinds of heat transmission ways, which are convection, conduction and radiation.

In the steady state, the equation of 3D heat conduction in the switch-gear is shown below:

$$\lambda(\frac{\partial^2 T}{\partial x^2}+\frac{\partial^2 T}{\partial y^2}+\frac{\partial^2 T}{\partial z^2})=-q \tag{15}$$

where T is the temperature, q is the energy generated per unit volume, λ is the heat conductivity coefficient.

C. EQUATIONS OF FLUID FIELD

In the simulations of this paper, the C-GIS is assumed to be in normal operation. Based on the mass conservation equation, the momentum conservation equation and the energy conservation equation, the basic Navier-Stokes flow field equations can be derived.

The mass conservation equation is shown below:

$$\frac{\partial \rho}{\partial t}+\nabla\cdot(\rho \boldsymbol{v})=0 \tag{16}$$

This equation can describe various type of fluid including Newtonian fluid and non-newton fluids.

Every fluid system has to follow the momentum conservation equation. This equation describes the phenomenon that the gradient of the momentum of the fluid equals to the resultant force put on the fluid. The Momentum conservation equations along x, y and z directions are shown below:

$$\frac{\partial(\rho u)}{\partial t}+\nabla\cdot(\rho u\mathbf{u})=\nabla\cdot(\eta\nabla u)-\frac{\partial p}{\partial x}+s_u \tag{17}$$

$$\frac{\partial(\rho v)}{\partial t}+\nabla\cdot(\rho v\mathbf{u})=\nabla\cdot(\eta\nabla v)-\frac{\partial p}{\partial y}+s_v \tag{18}$$

$$\frac{\partial(\rho w)}{\partial t}+\nabla\cdot(\rho w\mathbf{u})=\nabla\cdot(\eta\nabla w)-\frac{\partial p}{\partial z}+s_w \tag{19}$$

where S_u, S_v and S_w can be described as:

$$s_u=\frac{\partial}{\partial y}(\eta\frac{\partial v}{\partial x})+\frac{\partial}{\partial z}(\eta\frac{\partial u}{\partial x})+\frac{1}{3}\frac{\partial}{\partial x}(\eta\frac{\partial u}{\partial x})-\frac{2}{3}\frac{\partial}{\partial x}(\eta(\frac{\partial v}{\partial y}+\frac{\partial w}{\partial z})) \tag{20}$$

$$s_v=\frac{\partial}{\partial z}(\eta\frac{\partial v}{\partial y})+\frac{\partial}{\partial x}(\eta\frac{\partial w}{\partial y})+\frac{1}{3}\frac{\partial}{\partial y}(\eta\frac{\partial v}{\partial y})-\frac{2}{3}\frac{\partial}{\partial y}(\eta(\frac{\partial v}{\partial y}+\frac{\partial w}{\partial z})) \tag{21}$$

$$s_w=\frac{\partial}{\partial x}(\eta\frac{\partial u}{\partial z})+\frac{\partial}{\partial y}(\eta\frac{\partial v}{\partial z})+\frac{1}{3}\frac{\partial}{\partial z}(\eta\frac{\partial w}{\partial z})-\frac{2}{3}\frac{\partial}{\partial z}(\eta(\frac{\partial u}{\partial x}+\frac{\partial v}{\partial y})) \tag{22}$$

In above equations, u, v, w are respectively the gas velocities along x, y and z directions. ρ is the gas density, ρ is the viscosity coefficient of gas. For any fluid system that includes the heat transmission, they must follow the energy conservation equation. The energy conservation equation is shown below.

$$\frac{\partial(\rho h)}{\partial t}+\nabla\cdot(\rho h\mathbf{u})=\nabla\cdot(\frac{\lambda}{c_p}\nabla h)+S_h \tag{23}$$

In this paper, the only energy source for the fluid is the heat transmission with the solid components. The electromagnetic loss generated by the conductors leads to the rise of its own temperature and continuously transfer to other components through solid-solid and fluid-solid interface. The heat transmission is significantly influenced by the electromagnetic loss and the structure of switch-gear which has a significant impact on the flow of the fluid.

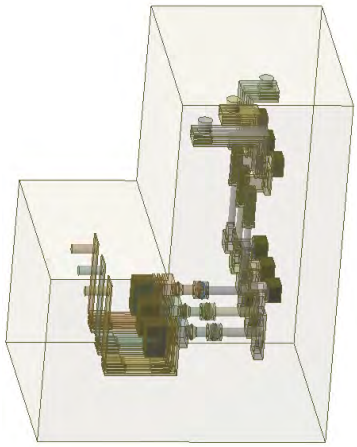

FIGURE 1. 1. 3D model of the C-GIS.

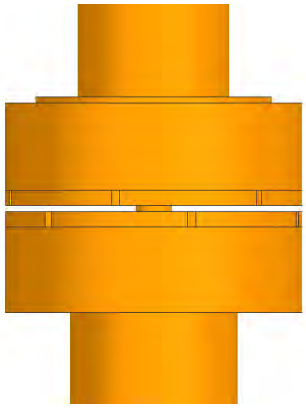

FIGURE 2. The contact resistance model between the fixed and moving contacts.

III. 3D MODEL OF 40.5KV C-GIS

The model of the SF_6-insulated C-GIS is established in UG NX 10.0 software with the contact resistance between fixed and moving contact is taken into consideration. The vacuum interrupter is contained in the embedded pole which is composed of epoxy resin. The relative permeability of epoxy resin is approximately 1 and its coefficient of heat conduction is lower than 1, we ignored the epoxy resin components in the C-GIS for it has little influence on the simulation of the eddy-current field and temperature field. To simulate the influence of the vacuum environment on the fixed and moving contacts, the interfaces between the contacts and the SF_6 gas is set as adiabatic to prevent the heat convection between the contacts and SF_6 gas. Other parts of the C-GIS are established in the same-size ratio. The overall model of the C-GIS is shown in Fig. 1. The C-GIS is formed by the upper and lower part which is separated by a clapboard. The rated current for this switch-gear is 2500A. The environment temperature is set

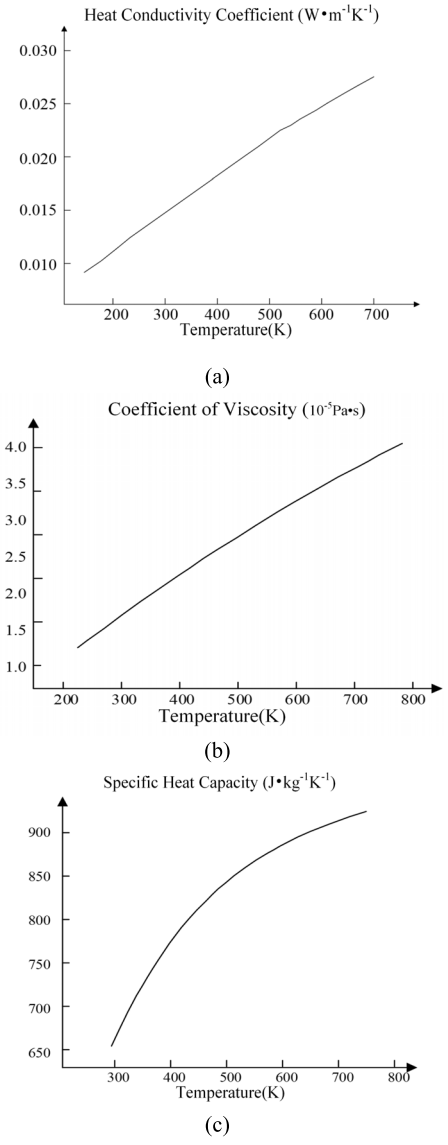

FIGURE 3. Physical characteristics of SF_6. (a) Temperature variation diagram of heat conductivity coefficient (b) Temperature variation diagram of coefficient of viscosity (c) Temperature variation diagram of specific heat capacity.

at 300K. The shell of vacuum interrupter is ignored in the simulation.

In order to acheive higher accuracy, contact resistance is taken into consideration. The fixed and moving contacts in the vacuum interrupter is made of CuCr50. A cylindroid model is added between the fixed and moving contacts, to simulate the contact resistance. The radius and length of the contact resistance cylinder can be determined by following equations:

$$R_c = K(0.102F)^{-m} \tag{24}$$

in which F is the pressure, K is a constant determined by the material, R_c is the contact resistance, m is a constant determined by the type of the contact, m is respectively 0.5 for point contact, 0.7 for line contact and 1 for surface contact.

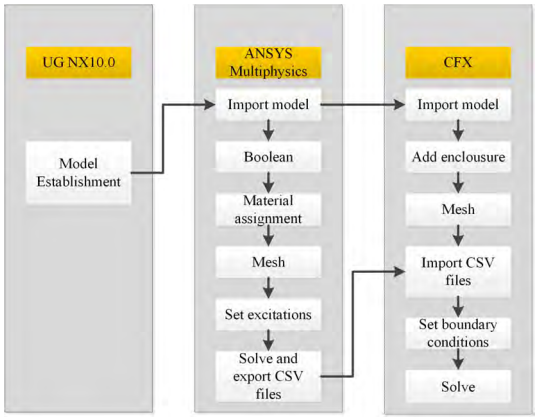

FIGURE 4. Process of ANSYS-CFX coupling simulation.

$$F = 0.6H\pi a^2 \tag{25}$$

in which H is the Brinell hardness of the material, a is the radius of the cylinder.

The vacuum interrupter used in the C-GIS can offer 3700N pressure and the Brinell hardness of CuCr50 is about 128. Combining (24) and (25), the contact resistance can be obtained, that is 1.65$\mu\Omega$. The 3D model of contact resistance between the fixed and moving contact is shown in Fig.2.

IV. PHYSICAL CHARACTERISTICS OF SF_6 GAS

The C-GIS analyzed in this paper is filled with pure SF_6 as insulation medium. SF_6 is a kind of highly electronegative gas, its molecule can adsorb free electron easily and weaken the impact ionization in the gas. For this reason, the dielectric strength of SF_6 gas is 2.5 times higher than air. Many researches have been done to analyze the temperature rise of SF_6-insulated equipment [7]–[9], in these simulations the physical property of SF_6 is set as constant which means ignoring the influence of temperature on the SF_6 gas. During the operation of the SF_6-insulated equipment, the SF_6 gas will be heated by the heat convection of the conductors which can leads to obvious temperature rise and change of physical property. This neglect of the variation of the physical properties of SF_6 gas caused by temperature can leads to a decrease in accuracy.

Noticed that the physical property parameters of SF_6 vary with temperature, we take the variation of the heat conductivity coefficient, coefficient of viscosity and constant-pressure specific heat capacity into consideration in this simulation for they have significant influence on the temperature rise of the C-GIS. With the increase of temperature, these three parameters are all on the rise. The temperature variation diagrams of these three parameters are shown in Fig. 3.

V. COUPLING SOLUTION METHOD

To conduct an Ansys-Cfx coupling simulation, the first step is to establish a 3D model in UG NX10.0. Then the model has to be imported to Ansys Multiphysics. In the section of Ansys

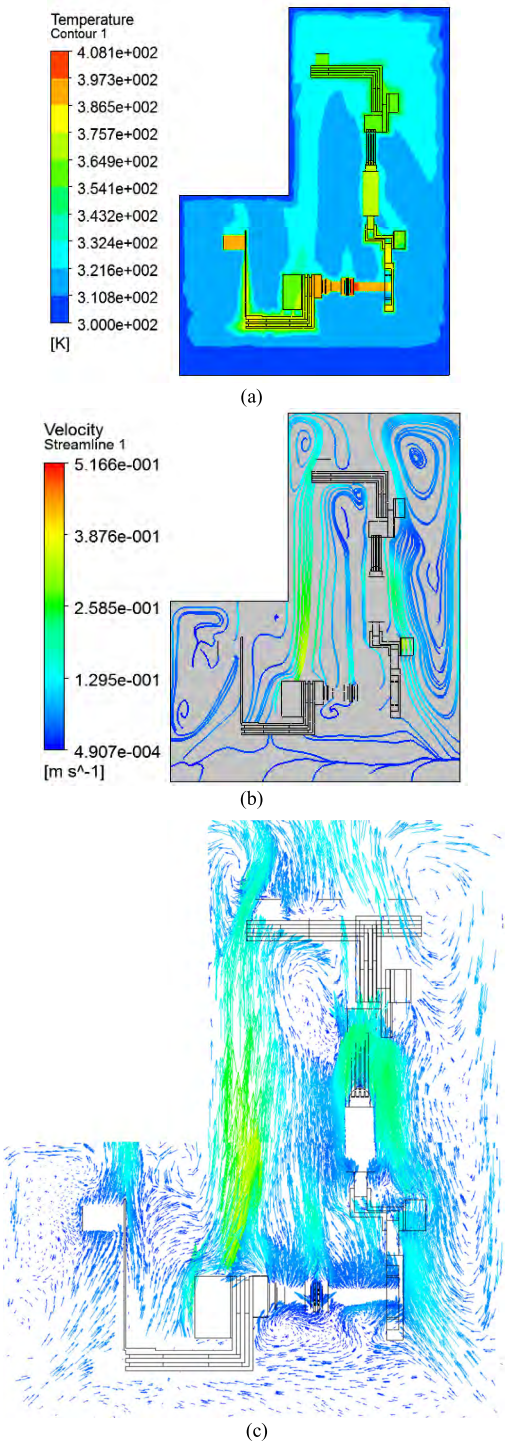

FIGURE 5. Simulation results of the C-GIS (a) Temperature distribution (b) Steamlines (c) Flow vector inside the C-GIS.

Multiphysics, operations such as booleans, material assignment, meshing and set of boundary conditions have to be done before the step of solving. After solution, the heat generated by electromagnetic loss will be recorded in CSV files. Then we import the CSV files into the Cfx as heat generation sources and finish the simulation. The process of Ansys-Cfx coupling simulation is shown in Fig.4.

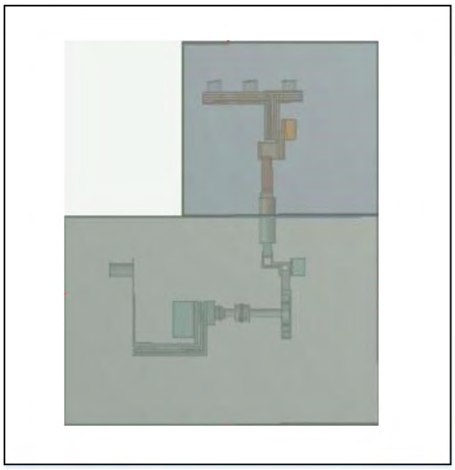

FIGURE 6. C-GIS and its surrounding air environment.

VI. SIMULATION RESULTS AND DISCUSSIONS

A. SIMULATION WITHOUT AIR ENVIRONMENT CONSIDERED

In the simulation, the fluid model in the simulation is set as ideal gas. The parameters of the gas are introduced into the simulation in the form of functions of temperature. The influence of gravity are also taken into consideration, the acceleration of gravity is set as 9.8m/s^2. The rate of convergence is set as 10^{-4} in the simulation. After 1000 steps of iteration, CFX achieves the convergence accuracy. The total computation time is about 8 hours.

Shown in Fig. 5(a) is the distribution of temperature of the C-GIS cross section provided by the simulation. From Fig. 5. it can be seen that the highest temperature inside the C-GIS is 408.1K which appears at the touch point of the moving and fixed contact inside the vacuum interrupter. This is because of the decrease of the sectional area of the conductor at the touch point, which leads to higher current density and higher resistance. Observing the global distribution of the temperature, it can be seen that with the increase of the distance away from the vacuum interrupter, the temperature of other parts decreases gradually. Besides, the cooling effect of the heat radiator is remarkable, the temperature of the components closed to radiators is lower. More heat is generated in the lower part of the C-GIS for more conductors contained there, so that the conductors in the lower part is of higher temperature. However, the upper part of the shell is of higher temperature for the rise of the hot-gas. Figure 5 (b) and (c) is the fluid streamlines and flow velocities of the C-GIS. It can be seen that the streamlines are more concentrated and fluid velocity is faster around the radiators which locates on the left of the fixed contact. Besides, it can be clearly seen that the SF_6 gas in the C-GIS generally rises. The velocity of the gas is slow, and a lot of vertexes are generated because the C-GIS is sealed. Figure 5(c) are the enlarged drawings of the flow velocities in the C-GIS, it can be obviously seen that fluid velocity is faster around

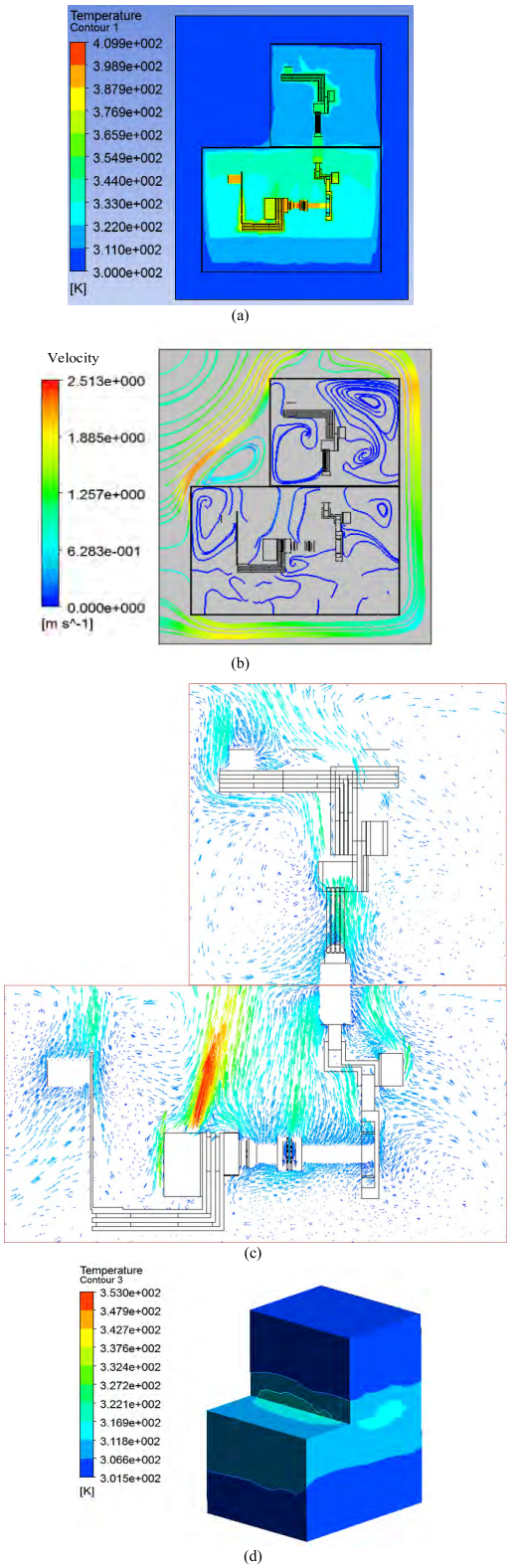

FIGURE 7. Simulation results of the C-GIS. (a) Temperature distribution (b) Streamlines (c) Flow vector (d) Temperature of the shell.

the radiators because that the temperature of gas around the conductors is higher, which accelerates the molecular movement.

FIGURE 8. Experiment setup.

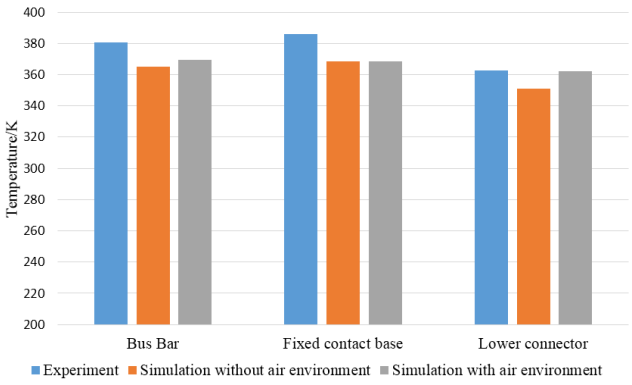

FIGURE 9. Results of the experiment and simulations.

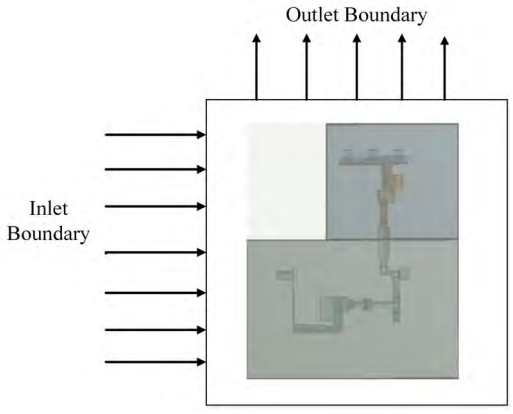

FIGURE 10. Simulation model of the cooling system.

B. SIMULATION WITH AIR ENVIRONMENT CONSIDERED

In above section, the air environment around the C-GIS is ignored and its influence on the C-GIS is simulated by setting boundary conditions on the shell of the C-GIS. In this section,

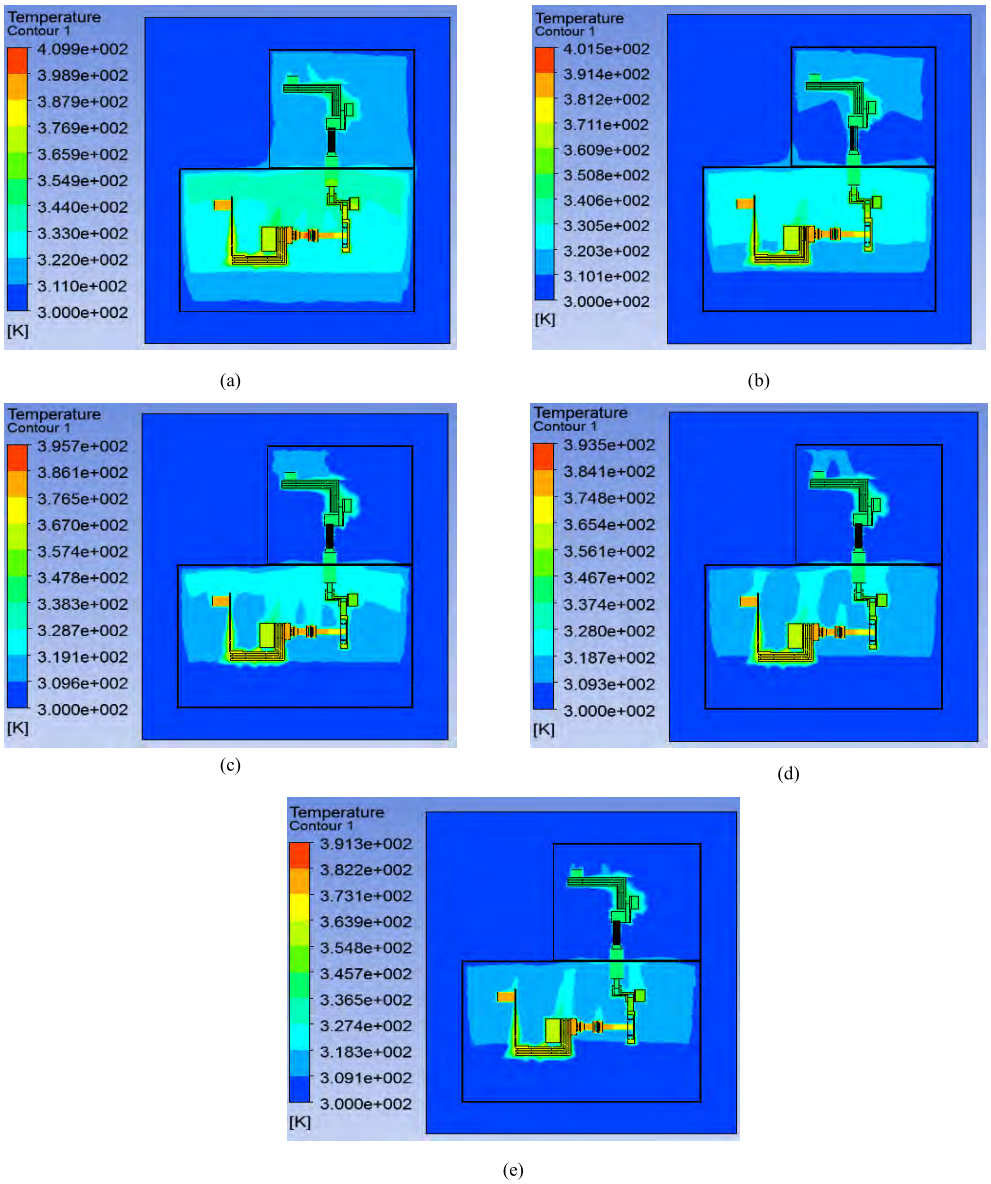

FIGURE 11. **Temperature distribution under different inlet velocity. (a) 1m/s. (b) 4m/s. (c) 5.5m/s. (d) 7m/s. (e) 9m/s.**

the air environment is taken into consideration and is set as ideal air model. Besides, the whole C-GIS is divided into the upper and lower part, which is more close to the real situation. The boundary condition around the air environment is set as wall with temperature set as 300K. The outlet boundary is set at the upper surface of the air domain, the relative pressure is set as 0 Pa to simulate the natural convection at room temperature. Figure 6 is the diagram of the air environment and the C-GIS.

After simulation, the distribution of temperature and fluid field is shown in Fig. 7 (a)-(d).

Taken the air environment into consideration, the simulation is more precise. Compared to the former simulation, the highest temperature in the C-GIS increases to 409.9K. The distribution of temperature is of little difference compared to that without air environment considered. The highest temperature is still at the touch point of the moving and fixed contact. This is because of the decrease of the

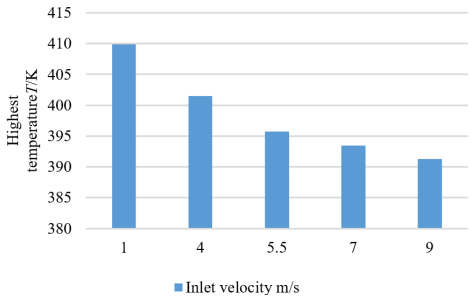

FIGURE 12. **The histogram of the inlet velocity and the highest temperature.**

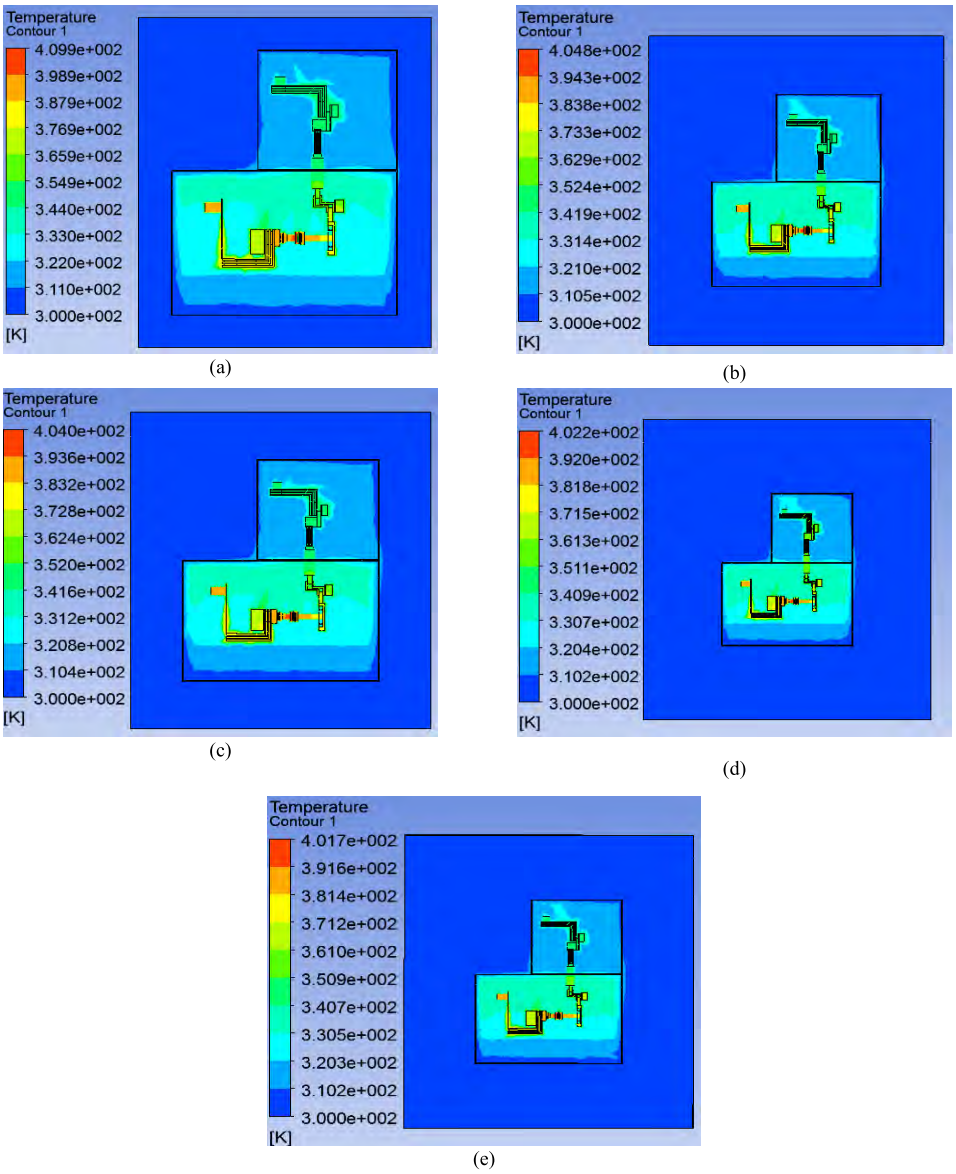

FIGURE 13. Temperature distribution with different distance from barriers. (a) 20cm. (b) 35cm. (c) 50cm. (d) 65cm. (e) 80cm.

sectional area of the conductor, which leads to higher current density and higher resistance. The effect of the radiator is still remarkable, the temperature of the components closed to radiators is lower. In the air environment outside of the C-GIS, forced convection is used to simulate the environmental wind speed. Figure7 (d) is the temperature distribution of the shell of the C-GIS, the highest temperature of the shell is at the junction of the upper and lower part of the C-GIS.

C. COMPARISON WITH EXPERIMENTAL RESULTS

Temperature rise experiment of the C-GIS is conducted. In the experiment, thermocouples are used to measure the temperature in the C-GIS. The current is set at the rated value during the experiment. The experiment setup is shown in Fig. 8. Using the temperature of the bus bar of A phase as example, the experimental result is 380.64K, the simulation result without air environment considered is 365.2K and the simulation result with air environment considered is 369.4K. The simulation with air environment considered is more precise. The results of other components are shown in Fig. 9. From the results, it can be seen that the simulation result is close to the experimental result.

D. INFLUENCE OF COOLING SYSTEM

To reduce the temperature rise inside the C-GIS, applying cooling system is an effective way. Several simulations are set up to analyze the effect of cooling system. The simulation model we adopted is shown in Fig. 10. The boundary conditions of the simulations are set up to simulate the common draught fans. The outlet boundary is at the top surface of

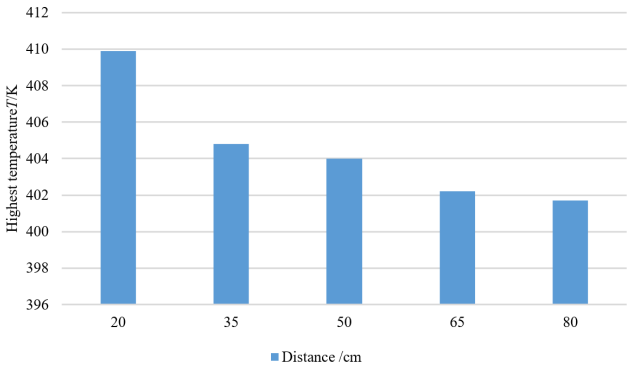

FIGURE 14. The histogram of the distance between the C-GIS and surrounding barriers and the highest temperature.

the air environment whose pressure is set as 0 Pa. The inlet boundary is of constant inlet velocity and is set at the left surface of the air environment. The other four surfaces are set as walls with temperature set as 300K.

In this section, five contrastive simulations with different inlet velocities are analyzed in order to simulate the influence of the cooling system. The inlet velocity of the five contrastive simulations are respectively set as 1m/s, 4m/s, 5.5m/s, 7m/s and 9m/s. The Fig. 11. (a)-(e) is the distribution of temperature in the C-GIS under different inlet velocity.

From Fig.11, it can be seen that the highest temperature in these simulations is respectively 409.9K, 401.5K, 395.7K, 393.5K and 391.3K, which all locates at the contact of the fixed and moving contact. The distribution of temperature is similar, this indicates that although the change of inlet velocity influences the heat dissipation of the C-GIS, the heat generated by the conductors is still the same. With the increase of the inlet velocity, the temperature of SF_6 gas is decreasing, which leads to better heat convection and lower temperature rise. The histogram of the inlet velocity and the highest temperature is shown in Fig.12.

Along with the increase of the inlet velocity, the temperature decreases and the distribution of high-temperature gas reduces. When the inlet velocity is lower than 4m/s, the temperature decreases sharply along with the increase of inlet velocity. But when the inlet velocity is higher than 4m/s, the decrease of temperature becomes slower. This is because of when the inlet velocity reaches a certain value, the heat dissipation effect of the forced convection has reached a limitation, after which the temperature rise cannot be reduced dramatically by increasing inlet velocity alone. Comparing the temperature rise of the C-GIS with and without cooling system, we can conclude that the cooling system is of great use in the mitigation of temperature rise.

E. INFLUENCE OF SURROUNDING BARRIERS

In the actual use of the C-GIS, the heat dissipation of the C-GIS is also influenced by the surrounding barriers. For instance, if the C-GIS is too close to a wall, its heat dissipation will worsen. In this section, contrastive simulations are established to analyze the influence of the distance between C-GIS and surrounding barriers on the temperature rise of C-GIS.

Five contrastive simulations are established in this paper. The distance between C-GIS and surrounding barriers in these simulations are respectively 20cm, 35cm, 50cm, 65cm and 80cm. The surfaces of the air environment are set as wall of 300K to simulate the surrounding barriers. With the boundary conditions set the same, the temperature distribution of these simulations are shown in Fig. 13. (a)-(e).

The highest temperature in the C-GIS of different distance is respectively 409.9K, 404.8K, 404.0K, 402.2K and 401.7K. It can be seen that along with the increase of the distance, the highest temperature decreases. When the distance is lower than 50cm, the highest temperature in the C-GIS decreases sharply. When the distance is higher than 50cm, the decrease of the highest temperature is small. This is because a balance between the C-GIS and air environment has been established when the distance is higher than 50cm. It can be concluded that the distance between the C-GIS and surrounding barriers is suitable to be set at about 50cm. The histogram of the distance between the C-GIS and surrounding barriers and the highest temperature is shown in Fig. 14.

VII. CONCLUSIONS

In this paper, electromagnetic-temperature-fluid coupling model is established. With the physical characteristics of SF_6set as temperature-varying, the temperature distribution, fluid velocity and streamlines are analyzed. Both simulations with and without air environment considered are established, the simulation results are then compared. After this, in order to optimize the heat dissipation of the C-GIS, the influence of cooling system and surrounding barriers are analyzed. The following conclusions can be drawn.

(1) Through electromagnetic-temperature-fluid coupling simulation of C-GIS, the distribution of temperature and flow field inside the C-GIS is obtained. The simulation result of temperature is in agreement with the experimental result. The highest temperature is both located at the touch point of the moving and fixed contact in vacuum interrupters. The effect of the radiator is still significant, the temperature of the components closed to radiators is lower. The SF_6 gas with higher temperature is generally going up toward top of C-GIS.

(2) Simulation results of C-GIS with cooling system show that cooling system is effective to reduce temperature rise of the C-GIS. It can be found that when the inlet velocity is lower than 4m/s, the temperature decreases sharply along with the increase of inlet velocity. But when the inlet velocity is higher than 4m/s, the decrease of temperature become slower.

(3) Simulation results with surrounding barrier show that the highest temperature decreases with the increase of the distance. When the distance is lower than 50cm, the highest temperature in the C-GIS decreases sharply. When the distance is higher than 50cm, the decrease of the highest temperature is little.

REFERENCES

[1] Y. Kawase, T. Ichihashi, and S. Ito, "Heat analysis of thermal overload relays using 3-D finite element method," *IEEE Trans. Magn.*, vol. 35, no. 3, pp. 1658–1661, May 1999.
[2] J. Paulke, H. Weichert, and P. Steinhauser, "Thermal simulation of switchgear," *Proc. 47th Holm Conf. Elect. Contacts*, Sep. 2001, pp. 6–11.
[3] A. Monnier, B. Froidurot, C. Jarrige, P. Testé, and R. Meyer, "A mechanical, electrical, thermal coupled-field simulation of a sphere-plane electrical contact," *IEEE Trans. Compon. Packag. Technol.*, vol. 30, no. 4, pp. 787–795, Dec. 2007.
[4] M. Clemens, E. Gjonaj, P. Pinder, and T. Weiland, "Numerical simulation of coupled transient thermal and electromagnetic fields with the finite integration method," *IEEE Trans. Magn.*, vol. 36, no. 4, pp. 1448–1452, Jul. 2000.
[5] V. Mateev, R. Tanev, and I. Marinova, "Simulation of electric and thermal fields of high voltage interrupter vacuum chamber," in *Proc. 18th Int. Symp. Elect. App. Technol.*, May 2014, pp. 1–4.
[6] J. K. Kim, S. C. Hahn, K. Y. Park, H. K. Kim, and Y. H. Oh, "Temperature rise prediction of EHV GIS bus bar by coupled magnetothermal finite element method," *IEEE Trans. Magn.*, vol. 41, no. 5, pp. 1636–1639, May 2005.
[7] S. Pawar, K. Joshi, L. Andrews, and S. Kale, "Application of computational fluid dynamics to reduce the new product development cycle time of the SF_6 gas circuit breaker," *IEEE Trans. Power Del.*, vol. 27, no. 1, pp. 156–163, Jan. 2012.
[8] X. W. Wu, N. Q. Shu, H. T. Li, and L. Li, "Contact temperature prediction in three-phase gas-insulated bus bars with the finite-element method," *IEEE Trans. Magn.*, vol. 50, no. 2, pp. 277–280, Feb. 2014.
[9] M. T. Dhotre, J. Korbel, X. Ye, J. Ostrowski, S. Kotilainen, and M. Kriegel, "CFD simulation of temperature rise in high-voltage circuit breakers," *IEEE Trans. Power Del.*, vol. 32, no. 6, pp. 2530–2536, Dec. 2017.
[10] L. Wang, W. Zheng, L. Wang, J. Lin, X. Li, and S. Jia, "Electromagnetic-thermal-flow field coupling simulation of 12-kV medium-voltage switchgear," *IEEE Trans. Compon. Packag. Manuf. Technol.*, vol. 6, no. 8, pp. 1208–1220, Aug. 2016.
[11] L. Wang, X. Li, J. Lin, and S. Jia, "Studies of modeling and simulation method of temperature rise in medium-voltage switchgear and its optimum design," *IEEE Trans. Compon. Packag. Manuf. Technol.*, vol. 8, no. 3, pp. 439–446, Mar. 2018.

LIJUN WANG received the B.S. degree in electrical engineering from Xi'an Jiaotong University, in 1997, the M.S. degree in electrical engineering from the Shenyang University of Technology, in 2002, and the Ph.D. degree in electrical engineering from Xi'an Jiaotong University, in 2006. From 1997 to 1999, he was with the Xi'an High-Voltage Apparatus Research Institute, where he was engaged in Research and Development of vacuum interrupter and circuit breaker. From 2009 to 2010, he was a Research Scholar with the Institutes of Research of Electronics and Applied Physics, University of Maryland, College Park. He is currently a Professor with the State Key Laboratory of Electrical Insulation and Power Equipment and Department of Electrical Engineering, Xi'an Jiaotong University. He is involved in the research of modeling and simulation of vacuum arcs and discharge plasmas, temperature rise simulation and partial discharge detection of electrical switchgears, vacuum dc breaking technology, and atmospheric-pressure plasma processing.

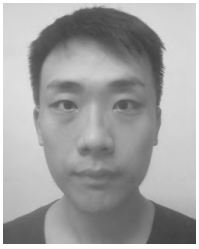

RUI WANG received the B.S. degree in electrical engineering from Xi'an Jiaotong University, Xi'an, in 2017, where he is currently pursuing the M.S. degree with the Department of Electrical Engineering. His current research interests include the simulation of medium voltage switchgear.

XIAOLIN LI received the B.S. degree in electrical engineering from Xidian University, Xi'an, China, in 2015, where he is currently pursuing the M.S. degree with the Department of Electrical Engineering. His current research interests include the simulation of medium voltage switchgear.

CHAO YAN received the B.S. degree in electrical engineering from the Dalian University of Technology, Dalian, China, in 2018. He is currently pursuing the M.S. degree with the Department of Electrical Engineering, Xi'an Jiaotong University, Xi'an. His current research interests include the on-line monitoring technology of medium voltage switchgear.